

Finite Difference Algorithm on Non-uniform Meshes for Modeling 2D Magnetotelluric Responses

Xiaozhong Tong^{1,2}, Yujun Guo¹, and Wei Xie¹

¹*School of Geosciences and Info-physics, Central South University, Changsha 410083, China*

²*Key Laboratory of Metallogenic Prediction of Nonferrous Metals of Ministry of Education, Central South University, Changsha 410083, China*

Correspondence should be addressed to Wei Xie; csumaysnow@csu.edu.cn

Abstract

A finite-difference approach with non-uniform meshes was presented for simulating magnetotelluric responses in 2D structures. We presented the formulation of this scheme and gave some sights into its successful implementation, and compared finite-difference solution with known numerical results and simple analytical solutions. First, a homogeneous half-space model was tested and the finite-difference approach can provide very good accuracy for 2D magnetotelluric modeling. Then we compared to the analytical solutions for the two-layered model, the relative errors of the apparent resistivity and the impedance phase were both increased when the frequency was increased. In the end, we compare our finite-difference simulation results with COMMEMI 2D-0 model with the finite-element solutions. Both results are in close agreement to each other. These comparisons confirm the validity and reliability of our finite-difference algorithm.

Keywords: finite-difference algorithm; magnetotelluric; 2D structures; modeling

1. Introduction

The magnetotelluric method is a passive electromagnetic exploration technique that measures orthogonal components of the electric and magnetic fields on the Earth's surface [1]. The source field is naturally generated by variations in Earth's magnetic field, which provide a wide and continuous spectrum of electromagnetic field waves. These fields induce currents into the Earth, which are measured at the surface and contain information about subsurface resistivity structures. With rapid advances in modeling and inversion, the magnetotelluric method has become one of the most important tools for geophysical exploring [2-3].

The magnetotelluric forward modeling aims to solve the frequency-domain Maxwell's equations and simulate the spatial and temporal distribution of electric and magnetic fields in the subsurface for a given conductivity distribution and a range of frequencies. Numerical modeling approaches such as finite difference (FD), finite element (FE), have been developed and applied as the process of forward calculation for 2D magnetotelluric

inversion [4-8]. The FD method based upon the differential form of the partial differential equations to be solved. Each derivative is replaced with an approximate difference formula and the computational domain is usually divided into rectangular cells. The efficiency and accuracy of the FD method for modeling magnetotelluric responses were proven for the 2D geo-electric model [9-10]. The FE method is another numerical technique that is often used for 2D and 3D magnetotelluric modeling, which involves assumed functional forms for the model and fields in small regions of specified geometry [11-14]. The FE method is accurate for real-world complex modeling, especially topography and bathymetry, because of the greater flexibility of mesh discretization. Meanwhile, there are some different approaches to the numerical approximation of 2D magnetotelluric forward problem [15-18]. There are a lot of good reviews of these methods about their advantages and disadvantages [19-20]. We refer to them in here for general view on the magnetotelluric modeling.

In this paper, a non-uniform meshes approach in FD numerical method was presented for general 2D magnetotelluric modeling. The main challenge in applying the method for solving the magnetotelluric boundary value problem is to calculate spatial derivatives. To verify the accuracy of the FD forward algorithm, the resulting numerical was compared to both an analytical solutions and the FE numerical solutions.

2. Governing equations

2.1. Electromagnetic equations. Considering a right-handed coordinate system, with z -axis pointing downwards and x -axis along geologic strike, and assuming time dependence as $e^{-i\omega t}$ and neglecting displacement currents, Maxwell's equations can be expressed in the frequency domain as [21]

$$\nabla \times \mathbf{E} = i\omega\mu\mathbf{H}, \quad (1)$$

$$\nabla \times \mathbf{H} = \sigma\mathbf{E}. \quad (2)$$

where \mathbf{E} is electric field and \mathbf{H} is magnetic field. ω is an angular frequency ($\omega = 2\pi/T$, T is a period). μ is the magnetic permeability in free space and $\mu = \mu_0 = 4\pi \times 10^{-7}$ H/m. σ is the electric conductivity in (S/m) and is varied only the direction of y -axis and z -axis, i.e., $\sigma = \sigma(y, z)$.

For a 2D conductivity structure assuming the x -axis is the geo-electrical strike direction (i.e., $\partial\mathbf{E}/\partial x \equiv 0$ and $\partial\mathbf{H}/\partial x \equiv 0$), expanding the curl operators in equation (1) and equation (2), the governing Maxwell's equations are given by

$$\begin{cases} \frac{\partial E_z}{\partial y} - \frac{\partial E_y}{\partial z} = i\omega\mu H_x, \\ E_y = \frac{1}{\sigma} \frac{\partial H_x}{\partial z}, \\ E_z = -\frac{1}{\sigma} \frac{\partial H_x}{\partial y}. \end{cases} \quad \text{TM-mode} \quad (3)$$

and

$$\begin{cases} \frac{\partial H_z}{\partial y} - \frac{\partial H_y}{\partial z} = \sigma E_x, \\ H_y = \frac{1}{i\omega\mu} \frac{\partial E_x}{\partial z}, \\ H_z = -\frac{1}{i\omega\mu} \frac{\partial E_x}{\partial y}. \end{cases} \quad \text{TE-mode} \quad (4)$$

These two modes are commonly referred to as transverse magnetic (TM) mode and transverse electric (TE) mode. We simulate the magnetic field H_x (TM-mode) or electric field E_x (TE-mode) parallel to the strike of the conductivity structure. According to equation (3) and equation (4), the associated partial differential equations can be written as

$$\frac{\partial}{\partial y} \left(\frac{1}{\sigma} \frac{\partial H_x}{\partial y} \right) + \frac{\partial}{\partial z} \left(\frac{1}{\sigma} \frac{\partial H_x}{\partial z} \right) + i\omega\mu H_x = 0, \quad (5)$$

$$\frac{\partial}{\partial y} \left(\frac{1}{i\omega\mu} \frac{\partial E_x}{\partial y} \right) + \frac{\partial}{\partial z} \left(\frac{1}{i\omega\mu} \frac{\partial E_x}{\partial z} \right) + \sigma E_x = 0. \quad (6)$$

According to these relations, the magnetotelluric impedances for the TM and TE modes are

$$Z_{yx} = Z_{TM} = \frac{E_y}{H_x}, \quad Z_{xy} = Z_{TE} = \frac{E_x}{H_y}. \quad (7)$$

The associated apparent resistivities and phases can be computed as

$$\rho_{a,ij} = \frac{1}{\omega\mu} |Z_{ij}|^2, \quad ij = xy, \quad ij = yx, \quad (8)$$

$$\phi_{ij} = \arctan \left[\frac{\text{Im}(Z_{ij})}{\text{Re}(Z_{ij})} \right]. \quad (9)$$

2.2. Boundary conditions. Within geo-electromagnetic induction we consider fields which change sufficiently slow, so that their variation in time is negligible compare to the duration of observation. In other words, we are more interested in their spatial distribution rather than their variation in time. Hence, this kind of forward problem belongs to boundary value problem, if the mathematical nomenclature is used.

For the TE-mode, the computational domain is composed of both the air space and the earth domain. For the TM-mode, the magnetic field H_x is nearly unchanged in the air space, so the air space can be eliminated from the computational domain [22]. To complete the boundary problem of the H -polarization, we must supply the boundary conditions for the magnetic field component on the outer boundaries. We restrict the computational domain for equation (5) and equation (6) to 2D bounded domain $\Omega = [y_{\min}, y_{\max}] \times [z_{\min}, z_{\max}]$, as shown in Figure 1. The computational domain is reduced to an isolated rectangular block with suitable boundary conditions. Then, we can divide the boundary of the computational domain Ω into four parts expressed as follows: $\Gamma_1 = \{(y, z) | y_{\min} < y < y_{\max}, z = z_{\min}\}$, $\Gamma_2 = \{(y, z) | z_{\min} < z < z_{\max}, y = y_{\min}\}$, $\Gamma_3 = \{(y, z) | z_{\min} < z < z_{\max}, y = y_{\max}\}$, and $\Gamma_4 = \{(y, z) | y_{\min} < y < y_{\max}, z = z_{\max}\}$. We impose Dirichlet Γ_1 , Neumann Γ_2 , Neumann Γ_3 , and Robin Γ_4

boundary conditions on the computational domain.

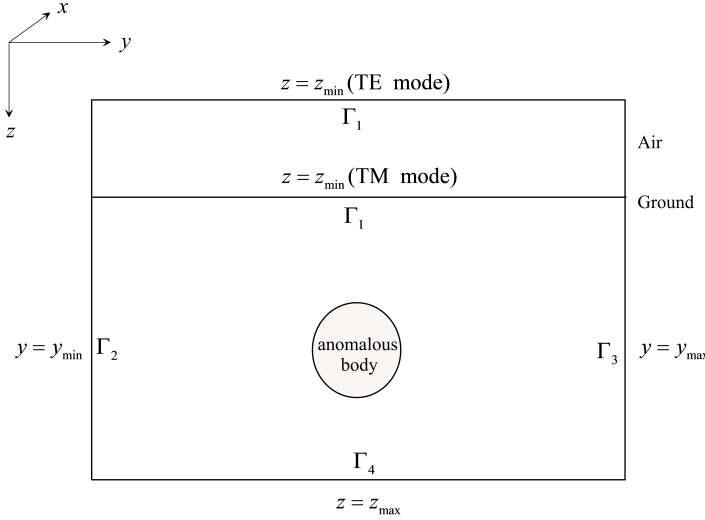


FIGURE 1: A sketch of computational domain for modeling 2D magnetotelluric responses.

3. Forward algorithm

3.1. FD representation for 2D magnetotelluric problem. Before we can solve equation (5) and equation (6), it is necessary to split the investigation area into a mesh with $(N_{zb} + N_{za}) \times N_y$ cells, where N_y is the number of cells in the horizontal direction and N_{zb} and N_{za} denote the number of cells in the vertical direction for the subsurface and the air, respectively. A resistivity value is assigned to each cell.

The FD approximation is the simplest form of electromagnetic modeling. In order to construct FD scheme for solving equation (5) and equation (6), non-uniform meshes shown in Figure 2 are constructed. In the TM-mode, approximation of second-order derivatives for equation (5) can be expressed as

$$\begin{aligned} \left[\frac{\partial}{\partial y} \left(\sigma \frac{\partial u}{\partial y} \right) \right]_{i,j} &\approx \frac{1}{\Delta y_i + \Delta y_{i+1}} \left[\left(\sigma \frac{\partial u}{\partial y} \right)_{i+1,j} - \left(\sigma \frac{\partial u}{\partial y} \right)_{i,j} \right] \\ &\approx \frac{\frac{\sigma_{i,j} + \sigma_{i+1,j}}{2} \frac{u_{i+1,j} - u_{i,j}}{\Delta y_i + \Delta y_{i+1}} - \frac{\sigma_{i-1,j} + \sigma_{i,j}}{2} \frac{u_{i,j} - u_{i-1,j}}{\Delta y_{i-1} + \Delta y_i}}{\frac{\Delta y_i + \Delta y_{i+1}}{2}} \\ &= \frac{2(\sigma_{i,j} + \sigma_{i+1,j})(u_{i+1,j} - u_{i,j})}{(\Delta y_i + \Delta y_{i+1})^2} - \frac{2(\sigma_{i-1,j} + \sigma_{i,j})(u_{i,j} - u_{i-1,j})}{(\Delta y_{i-1} + \Delta y_i)(\Delta y_i + \Delta y_{i+1})} \end{aligned} \quad (10)$$

and

$$\left[\frac{\partial}{\partial y} \left(\sigma \frac{\partial u}{\partial y} \right) \right]_{i,j} \approx \frac{2(\sigma_{i,j} + \sigma_{i,j+1})(u_{i,j+1} - u_{i,j})}{(\Delta z_j + \Delta z_{j+1})^2} - \frac{2(\sigma_{i,j-1} + \sigma_{i,j})(u_{i,j} - u_{i,j-1})}{(\Delta z_{j-1} + \Delta z_j)(\Delta z_j + \Delta z_{j+1})} \quad (11)$$

Substituting equation (10) and equation (11) into equation (5), the difference equation for TM-mode can be written as

$$\begin{aligned} & \frac{2(\sigma_{i,j} + \sigma_{i+1,j})(u_{i+1,j} - u_{i,j})}{(\Delta y_i + \Delta y_{i+1})^2} - \frac{2(\sigma_{i-1,j} + \sigma_{i,j})(u_{i,j} - u_{i-1,j})}{(\Delta y_{i-1} + \Delta y_i)(\Delta y_i + \Delta y_{i+1})} + \\ & \frac{2(\sigma_{i,j} + \sigma_{i,j+1})(u_{i,j+1} - u_{i,j})}{(\Delta z_j + \Delta z_{j+1})^2} - \frac{2(\sigma_{i,j-1} + \sigma_{i,j})(u_{i,j} - u_{i,j-1})}{(\Delta z_{j-1} + \Delta z_j)(\Delta z_j + \Delta z_{j+1})} + i\omega\mu u_{i,j} = 0 \end{aligned} \quad (12)$$

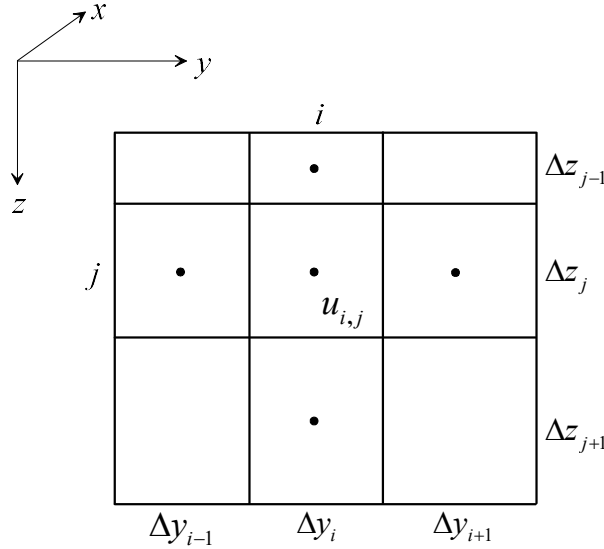


FIGURE 2: Discretization for 2D geo-electric model with non-uniform meshes.

In the TE-mode, the difference equation resulting from approximation of equation (6) is:

$$\begin{aligned} \left[\frac{\partial}{\partial y} \left(\frac{\partial u}{\partial y} \right) \right]_{i,j} & \approx \frac{1}{\Delta y_i + \Delta y_{i+1}} \left[\left(\frac{\partial u}{\partial y} \right)_{i+1,j} - \left(\frac{\partial u}{\partial y} \right)_{i,j} \right] \\ & \frac{u_{i+1,j} - u_{i,j}}{\Delta y_i + \Delta y_{i+1}} - \frac{u_{i,j} - u_{i-1,j}}{\Delta y_{i-1} + \Delta y_i} \\ & \approx \frac{2}{\Delta y_i + \Delta y_{i+1}} \end{aligned} \quad (13)$$

and

$$\left[\frac{\partial}{\partial z} \left(\frac{\partial u}{\partial z} \right) \right]_{i,j} \approx \frac{\frac{u_{i,j+1} - u_{i,j}}{\Delta z_j + \Delta z_{j+1}} - \frac{u_{i,j} - u_{i,j-1}}{\Delta z_{j-1} + \Delta z_j}}{\frac{2}{\Delta z_j + \Delta z_{j+1}}} \quad (14)$$

Therefore, substituting equations (13) and equation (14) into equation (6), the difference equation for TE-mode can be written as

$$\frac{\frac{u_{i+1,j} - u_{i,j}}{\Delta y_i + \Delta y_{i+1}} - \frac{u_{i,j} - u_{i-1,j}}{\Delta y_{i-1} + \Delta y_i}}{\frac{2}{\Delta y_i + \Delta y_{i+1}}} + \frac{\frac{u_{i,j+1} - u_{i,j}}{\Delta z_j + \Delta z_{j+1}} - \frac{u_{i,j} - u_{i,j-1}}{\Delta z_{j-1} + \Delta z_j}}{\frac{2}{\Delta z_j + \Delta z_{j+1}}} + i\omega\mu\sigma_{i,j}u_{i,j} = 0 \quad (15)$$

The solution vector \mathbf{u} , which represents the components H_x or E_x for the different mesh nodes, is rewritten by

$$\mathbf{u} = \begin{pmatrix} u_1 = u_{1,1} \\ u_2 = u_{1,2} \\ \vdots \\ u_{(i-1) \times (Ny+1) + j} = u_{i,j} \\ \vdots \\ u_{Nz \times (Ny+1) + Ny} = u_{Nz+1,Ny} \\ u_{(Nz+1) \times (Ny+1)} = u_{Nz+1,Ny+1} \end{pmatrix}, \quad (16)$$

Considering boundary conditions of the 2D magnetotelluric forward problem, the resulting linear system of equations in the form

$$\mathbf{K}\mathbf{u} = \mathbf{s}. \quad (17)$$

gives a numerical solution of equation (5) and equation (6). Where \mathbf{K} is the system matrix containing electrical parameters σ , and the right-side column vector \mathbf{s} contains information related to boundary conditions. Equation (17) can be solved by either a direct or iterative solver. Here, we use the direct solver for a sparse matrix in MATLAB to obtain the solution to equation (17). Finally, the magnetotelluric responses including impedances, apparent resistivity and phase at each site for each frequency are calculated by equation (8) and equation (9).

The subroutines described here for calculating magnetotelluric responses, given in [Appendix 1](#) and [Appendix 2](#), were developed in MATLAB without MATLAB's special toolboxes.

3.2. Benchmark with homogeneous half-space. To test the accuracy of our FD method, a homogeneous half-space model is illustrated for TM-mode. The size of computational domain was designed as 20 km \times 5 km. The earth's surface was assumed to be flat and homogeneous with a conductivity of 0.1 S/m. We supposed that there is one magnetotelluric site located on the surface ($z=0$ km). The magnetotelluric responses of the magnetic field H_x are computed in the frequency range 0.001 to 1000 Hz. The given domain was discretized into many elements and nodes with non-uniform approach. For information of mesh generation, the number of nodes in y -axis and z -axis are set as 51 and 41, respectively. The total numbers of nodes generated were 2091.

The results of the homogeneous half-space are shown in [Figure 3](#). It is obvious that the magnetic field H_x including its real part and imaginary part computed by the FD method with non-uniform meshes are good agree with the analytical solution. The results indicate that our FD approach can provide very good accuracy for 2D magnetotelluric modeling.

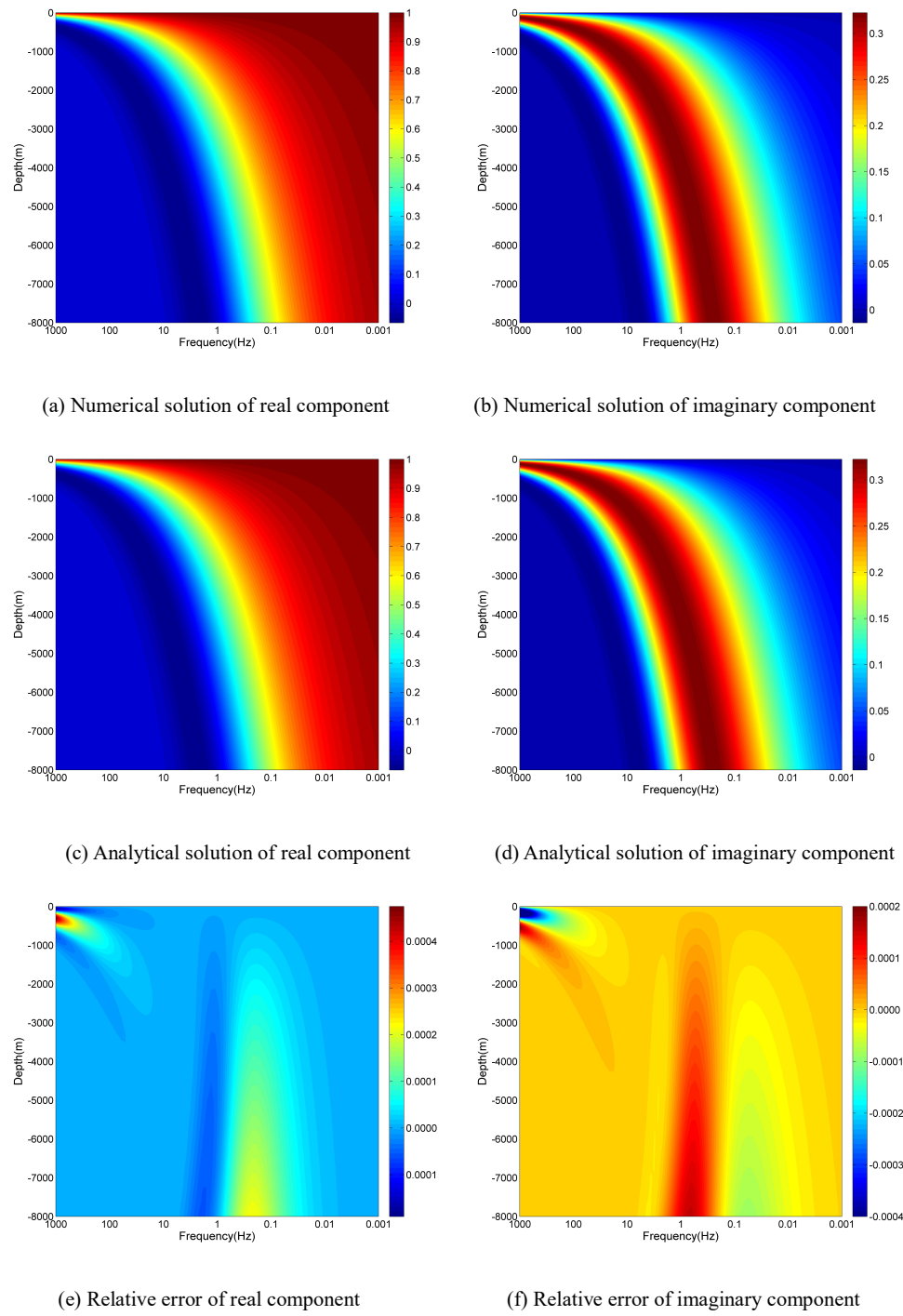


FIGURE 3: FD solution of magnetic field in homogeneous half-space model.

4. Numerical results

4.1. Comparison of FD results and analytical solutions. The two-layered model is used as an example for the comparison of FD numerical solution and analytical solution. It is supposed that the resistivity model includes two

layers. The thickness of the top layer 1 km, and its resistivity is assumed to be 10 ohm-m. For the bottom layer, its thickness and resistivity are assumed to be 1 km and 100 ohm-m. The size of the model is set as 20 km \times 2 km.

The results of the two-layered model are shown in Figure 4. It is obvious that relative errors of the apparent resistivity and the phase were both increased when the frequency was increased, with the maximum error at the longest frequency 1000 Hz and the minimum at the shortest frequency 0.001 Hz. At the highest frequency, the vertical grid spacing size at earth's surface must be small enough so that the linear approximation of the electric field is reasonably close to the exponential decay of the electromagnetic fields. Through the numerical examples, the first vertical mesh size should be suggested approximately 1/3 of the shortest skin depth of the top layer.

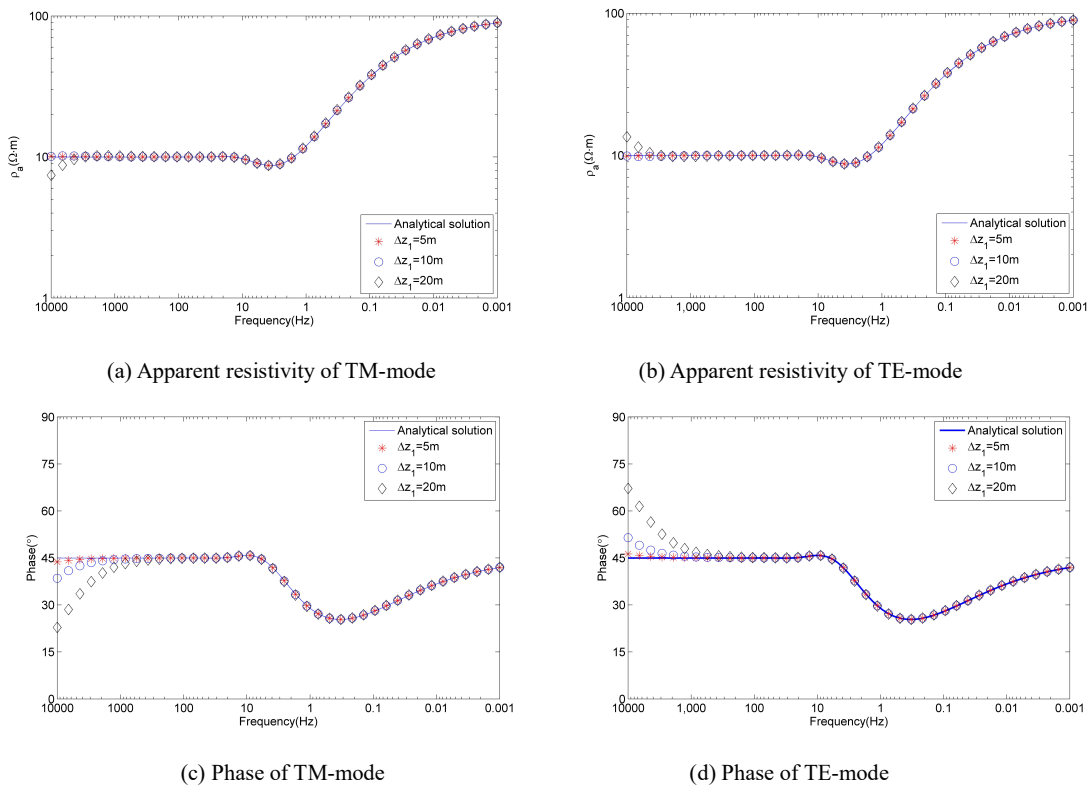


FIGURE 4: Comparison of FD solution and analytical solution for the two-layered model.

4.2. Comparison of FD results and FE solutions. In this section, the reliability of the non-uniform meshes FD algorithm is confirmed by testing on the COMMEMI 2D-0 model. The COMMEMI 2D-0 model, proposed by Zhdanov et al. for comparing of modeling methods for electromagnetic induction [23], is illustrated in Figure 5. It consists of three segments of different conductivities with horizontal contrasts of 1:10 and 2:1, lying on a perfectly conducting basement.

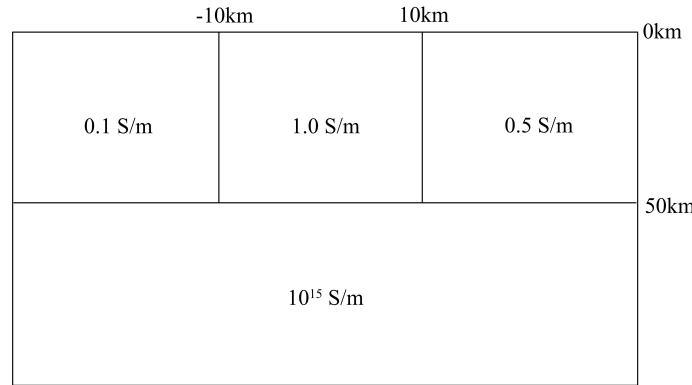


FIGURE 5: Schematic drawing of the COMMEMI 2D-0 model.

With a testing frequency of 0.033Hz, the calculated resistivities by the presented FD approach are compared with the FE solution [7] and the averaged volume integral results from the COMMEMI project [23]. The size of magnetotelluric domain was designed as 100 km \times 100 km. Using the technique of the non-uniform meshes, we set discrete elements in given domain as 100 \times 80 (i.e. $N_y=100$ and $N_z=80$), and extended 50km to air space for TE-mode. Figure 6 shows the results of the FD computations along a profile.

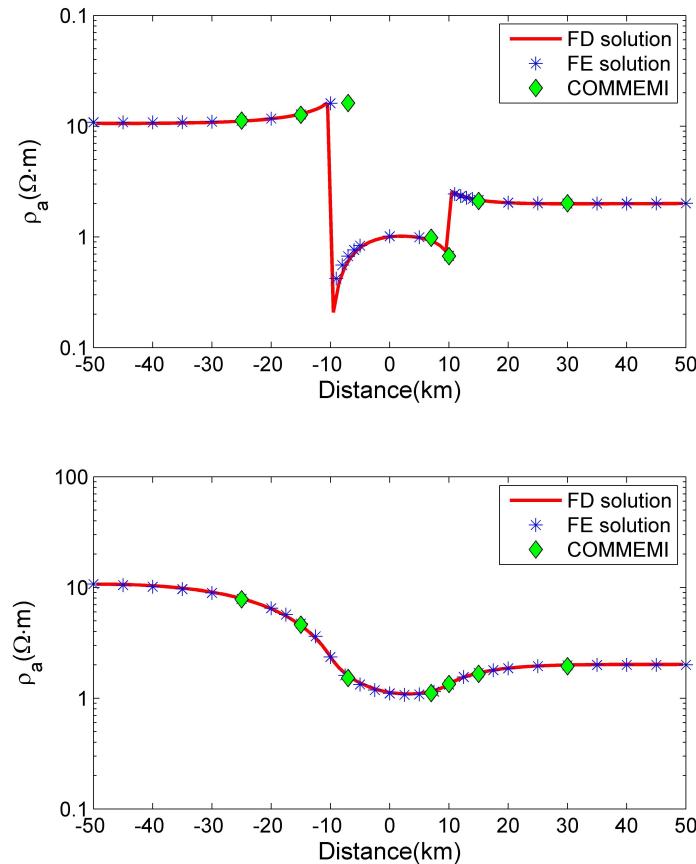


FIGURE 6: Comparison of FD solution and FE solution for the COMMEMI 2D-0 model. The upper figure displays the apparent resistivity of TM-mode, the lower figure the TE-mode.

One can see (Figure 6) that the results computed by the FD method and the FE method are in close agreement to each other. The apparent resistivities do not differ much. Compared to the FE solution, the average relative error for the apparent resistivity is 0.05, which are in the acceptance limits. Meanwhile, our results were quite comparable those of the COMMEMI 2D-0 projects.

5. Conclusions

The finite difference method with non-uniform meshes has been adapted to simulate the magnetotelluric responses of 2D earth conductivity structures. We presented the formulation of this scheme and gave some sights into its successful implementation. In a first investigation, a homogeneous half-space model was tested and the approach of non-uniform meshes can provide very good accuracy for 2D magnetotelluric modeling. Compared to the analytical solutions for the two-layered model, the relative errors of the apparent resistivity and the impedance phase were both increased when the frequency was increased. Meanwhile, the relative errors were reduced when the mesh size was reduced. The reason can be attributed that the accuracy of the FD calculation for the apparent resistivity and the impedance phase depends on the vertical grid spacing size near the surface. Furthermore, we presented the COMMEMI 2D-0 model in comparison to results derived by the FE calculation. Both results are in close agreement to each other. These comparisons confirm the validity and reliability of this FD algorithm.

Conflicts of Interest

The authors declared no potential conflicts of interest with respect to the research, authorship, and publication of this article.

Acknowledgements

This project is supported by National Natural Science Foundation of China grant (41674080) and Higher School Doctor Subject Special Scientific Research Foundation grant (20110162120064). The authors would like to thank the anonymous reviewers and editors for their helpful comments and improving the manuscript.

References

- [1] L. Cagniard, "Basic theory of the magneto-telluric method of geophysical prospecting," *Geophysics*, vol.18, no.3, pp.605-645, 1953.
- [2] T.J. Lee, N. Han, and Y. Song, "Magnetotelluric survey applied to geothermal exploration: An example at Seokmo Island, Korea," *Exploration Geophysics*, vol.41, no.1, pp.61-68, 2010.
- [3] H. Barcelona, A. Favetto, V.G. Peri, C. Pomposiello, and C. Ungarelli, "The potential of audiomagnetotellurics in the study of geothermal fields: A case study from the northern segment of the La Candelaria Range, northwestern Argentina," *Journal of*

Applied Geophysics, vol.88, no.1, pp.83-93, 2013.

- [4] C. deGroot-HedlinN and S. Constable, “Occam's inversion to generate smooth, two-dimensional models from magnetotelluric data,” *Geophysics*, vol.55, no.12, pp.1613-1624, 1990.
- [5] W. Rodi, and R.L. Mackie, “Nonlinear conjugate gradient algorithm for 2-D magnetotelluric inversion,” *Geophysics*, vol.66, no.1, pp.174-187, 2001.
- [6] W. Siripunvaraporn, and G.D. Egbert, “Data space conjugate gradient inversion for 2-D magnetotelluric data,” *Geophysical Journal International*, vol.170, no.3, pp.986-994, 2007.
- [7] S.K. Lee, H.J. Kim, Y. Song, and C.K. Lee, “MT2Dinvmatlab—a program in MATLAB and FORTRAN for two-dimensional magnetotelluric inversion,” *Computer & Geosciences*, vol.35, no.8, pp.1722-1734, 2009.
- [8] A. Kelbert, N. Meqbel, G.D. Egbert and K. Tandon, “ModEM: A modular system for inversion of electromagnetic geophysical data,” *Computers & Geosciences*, vol.66, pp.40-53, 2014.
- [9] J. Pek, and T. Verner, “Finite-difference modelling of magnetotelluric fields in two-dimensional anisotropic media,” *Geophysical Journal International*, vol.128, no.3, pp.505-521, 1997.
- [10] T. Kalscheuer, N. Juhojuntti, and K. Vaittinen, “Two-dimensional magnetotelluric modelling of Ore deposits: Improvements in model constraints by inclusion of borehole measurements,” *Surveys in Geophysics*, vol.39, no.3, pp.467-507, 2018.
- [11] P.E. Wannamaker, J.A. Stodt, and L. Rijo, “Two-dimensional topographic responses in magnetotellurics modeled using finite elements,” *Geophysics*, vol.51, no.11, pp.2131-2144, 1986.
- [12] A. Franke, R.U. Börner, and K. Spitzer, “Adaptive unstructured grid finite element simulation of two-dimensional magnetotelluric fields for arbitrary surface and seafloor topography,” *Geophysical Journal International*, vol.171, no.1, pp.71-86, 2007.
- [13] K. Key, and C. Weiss, “Adaptive finite-element modeling using unstructured grids: The 2D magnetotelluric example,” *Geophysics*, vol.71, no.6, pp.291-299, 2007.
- [14] W. Sarakorn, “2-D magnetotelluric modeling using finite element method incorporating unstructured quadrilateral elements,” *Journal of Applied Geophysics*, vol.139, no.1, pp.16-24, 2017.
- [15] J. Wittke, and B. Tezkan, “Meshfree magnetotelluric modelling,” *Geophysical Journal International*, vol.198, no.2, pp.1255-1268, 2014.
- [16] H.K. Du, Z.Y. Ren, and J.T. Tang, “A finite-volume approach for 2D magnetotellurics modeling with arbitrary topographies,” *Studia Geophysica et Geodaetica*, vol.60, no.2, pp.332-347, 2016.
- [17] A. Bihlo, C.G. Farquharson, R.D. Haynes, and J.C. Loredo-Osti, “Probabilistic domain decomposition for the solution of the two-dimensional magnetotelluric problem,” *Computational Geosciences*, vol.21, no.1, pp.117-129, 2017.
- [18] W. Sarakorn, and C. Vachiratienchai, “Hybrid finite difference-finite element method to incorporate topography and bathymetry for two-dimensional magnetotelluric modeling,” *Earth, Planets and Space*, vol.70, no.1, pp.70-103, 2018.
- [19] M.S. Zhdanov, I.M. Varentsov, J.T. Weaver, N.G. Golubev, and V.A. Krylov, “Methods for modelling electromagnetic fields

results from COMMEMI—the international project on the comparison of modelling methods for electromagnetic induction,” Journal of Applied Geophysics, vol.37, no.3, pp.133-271, 1997.

[20] D. Varilsoðlu, and M.E. Candansayar, “3D magnetotelluric modeling by using finite-difference method: Comparison study of different forward modeling approaches,” *Geophysics*, vol.83, no.2, pp.51-60, 2018.

[21] Z.Q. Guo, G.D. Egbert, and W.B. Wei, “Modular implementation of magnetotelluric 2D forward modeling with general anisotropy,” *Computer & Geosciences*, vol.118, pp.27-38, 2018.

[22] C. Aprea, J. Booker and J. Smith, “The forward problem of electromagnetic induction: Accurate finite-difference approximations for two-dimensional discrete boundaries with arbitrary geometry,” *Geophysical Journal International*, vol.129, no.1, pp.29-40, 1997.

[23] M.S. Zhdanov, I.M. Varentsov, J.T. Weaver, N.G. Golubev, V.A. Krylov, “Methods for modelling electromagnetic fields results from COMMEMI—the international project on the comparison of modelling methods for electromagnetic induction,” Journal of Applied Geophysics, vol.37, no.3, pp.133-271, 1997.

Appendix 1: MATLAB Program for simulating TE-mode responses

```

function [Ex,rho_a,phase]=MT2D_TE_FDM_Nonuniform(dy,dz_air,dz_earth,rho,fre)
% Input arguments

% dy: Mesh size in y direction
% dz_air: Mesh size in z direction (air)
% dz_earth: Mesh size in z direction (earth)
% rho: Mesh resistivity
% fre: Frequency

% Output
% Ex: Electric field
% rho_a: Apparent resistivity
% phase: Impedance phase

mu=4e-7*pi;
fre=logspace(-3,3,40);
dz=[dz_air dz_earth];
Ny=length(dy);
Nz_air=length(dz_air);
Nz_earth=length(dz_earth);
Nz=Nz_air+Nz_earth;

```

```
L=sparse(Ny*Nz,Ny*Nz);
R=sparse(Ny*Nz,1);
for nf=1:1:size(fre,2)
    % Formed linear equation
    % Inner nodes
    for i=2:1:Nz-1
        for j=2:1:Ny-1
            k=(j-1)*Nz+i;
            L(k,k-Nz)=4/((dy(j)+dy(j+1))*(dy(j-1)+dy(j)));
            L(k,k+Nz)=4/((dy(j)+dy(j+1))*(dy(j)+dy(j+1)));
            L(k,k-1)=4/((dz(i)+dz(i+1))*(dz(i-1)+dz(i)));
            L(k,k+1)=4/((dz(i)+dz(i+1))*(dz(i)+dz(i+1)));
            L(k,k)=sqrt(-1)*2*pi*fre(nf)*mu/rho(i,j)-...
                (4/((dy(j)+dy(j+1))*(dy(j-1)+dy(j)))+...
                4/((dy(j)+dy(j+1))*(dy(j)+dy(j+1)))-...
                (4/((dz(i)+dz(i+1))*(dz(i-1)+dz(i)))+...
                4/((dz(i)+dz(i+1))*(dz(i)+dz(i+1))));
            R(k,1)=0;
        end
    end
    % Upper boundary
    i=1;
    for j=1:1:Ny
        k=(j-1)*Nz+i;
        L(k,k)=1;
        R(k,1)=1;
    end
    % Lower boundary
    i=Nz;
    for j=1:1:Ny
        k=(j-1)*Nz+i;
        L(k,k)=1/dz(end)+sqrt(-1)*2*pi*fre(nf)*mu*(1/rho(i,j));
        L(k,k-1)=-1/dz(end);
    end
end
```

```
R(k,1)=0;  
end  
% Left boundary  
for i=1:1:Nz  
    for j=1:1:Ny  
        k=(j-1)*Nz+i;  
        if(j==1&&i>1&&i< Nz)  
            L(k,k)=1;L(k,k+Nz)=-1;  
            R(k,1)=0;  
        end  
    end  
end  
% Right boundary  
for i=1:1:Nz  
    for j=1:1:Ny  
        k=(j-1)*Nz+i;  
        if(j==Ny&&i>1&&i< Nz)  
            L(k,k)=1;L(k,k-Nz)=-1;  
            R(k,1)=0;  
        end  
    end  
end  
% Solving the linear equation  
u(:,nf)=L\R;  
u=full(u);  
u_new(:, :, nf)=reshape(u(:, nf), Nz, Ny);  
u1(:, nf)=u_new(Nz_air+1, :, nf);  
u2(:, nf)=u_new(Nz_air+2, :, nf);  
u3(:, nf)=u_new(Nz_air+3, :, nf);  
u4(:, nf)=u_new(Nz_air+4, :, nf);  
for i=1:1:Ny  
    ux(i,nf)=(-11*u1(i,nf)+18*u2(i,nf)-9*u3(i,nf)+2*u4(i,nf))...  
    /(2*3*dz(Nz_air+1));
```

```

Zyx(i,nf)=u1(i,nf)/((1/(sqrt(-1)*2*pi*fre(nf)*mu))*ux(i,nf));
rho_a(i,nf)=abs(Zyx(i,nf))^2/(2*pi*fre(nf)*mu);
phase(i,nf)=-atan(imag(Zyx(i,nf))/real(Zyx(i,nf)))*180/pi;
end
end
Ex=u_new;

```

Appendix 2: MATLAB Program for simulating TM-mode responses

```

function [Hx,rho_a,phase]=MT2D_TM_FDM_Nonuniform(dy,dz,rho,fre)
% Input arguments
% dy: Mesh size in y direction
% dz: Mesh size in z direction
% rho: Mesh resistivity
% fre: Frequency
% Output arguments
% Hx: Magnetic field
% rho_a: Apparenet resistivity
% phase: Impedance phase
mu=4e-7*pi;
Ny=length(dy);
Nz=length(dz);
L=sparse(Ny*Nz,Ny*Nz);
R=sparse(Ny*Nz,1);
for nf=1:1:size(fre,2)
    % Formed linear equation
    % Inner nodes
    for i=2:1:Nz-1
        for j=2:1:Ny-1
            k=(j-1)*Nz+i;
            L(k,k-Nz)=(rho(i,j-1)+rho(i,j))*2/((dy(j)+dy(j+1))*(dy(j-1)+dy(j)));
            L(k,k+Nz)=(rho(i,j+1)+rho(i,j))*2/((dy(j)+dy(j+1))*(dy(j)+dy(j+1)));
            L(k,k-1)=(rho(i-1,j)+rho(i,j))*2/((dz(i)+dz(i+1))*(dz(i-1)+dz(i)));
            L(k,k+1)=(rho(i+1,j)+rho(i,j))*2/((dz(i)+dz(i+1))*(dz(i)+dz(i+1)));
        end
    end
end

```

```
L(k,k)=sqrt(-1)*2*pi*fre(nf)*mu-...
(rho(i,j-1)+rho(i,j))*2/((dy(j)+dy(j+1))*(dy(j-1)+dy(j)))-...
(rho(i,j+1)+rho(i,j))*2/((dy(j)+dy(j+1))*(dy(j)+dy(j+1)))-...
(rho(i-1,j)+rho(i,j))*2/((dz(i)+dz(i+1))*(dz(i-1)+dz(i)))-...
(rho(i+1,j)+rho(i,j))*2/((dz(i)+dz(i+1))*(dz(i)+dz(i+1)));
R(k,1)=0;
end
end
% Upper boundary
i=1;
for j=1:1:Ny
k=(j-1)*Nz+i;
L(k,k)=1;
R(k,1)=1;
end
% Lower boundary
i=Nz;
for j=1:1:Ny
k=(j-1)*Nz+i;
L(k,k)=1/dz(end)+sqrt(-sqrt(-1)*2*pi*fre(nf)*mu*(1/rho(i,j)));
L(k,k-1)=-1/dz(end);
R(k,1)=0;
end
% Left boundary
for i=1:1:Nz
for j=1:1:Ny
k=(j-1)*Nz+i;
if(j==1&&i>1&&i<Nz)
L(k,k)=1;L(k,k+Nz)=-1;
R(k,1)=0;
end
end
end
```

```
% Right boundary
for i=1:1:Nz
    for j=1:1:Ny
        k=(j-1)*Nz+i;
        if(j==Ny&&i>1&&i<Nz)
            L(k,k)=1;L(k,k-Nz)=-1;
            R(k,1)=0;
        end
    end
end

% Solving the linear equation
u(:,nf)=L\R;
u=full(u);
u_new(:, :, nf)=reshape(u(:, nf), Nz, Ny);
u1(:, nf)=u_new(1, :, nf);
u2(:, nf)=u_new(2, :, nf);
u3(:, nf)=u_new(3, :, nf);
u4(:, nf)=u_new(4, :, nf);
for i=1:1:Ny
    ux(i, nf)=(-11*u1(i, nf)+18*u2(i, nf)-9*u3(i, nf)+2*u4(i, nf))/(2*3*dz(1));
    Zyx(i, nf)=rho(1, i)*ux(i, nf)/u1(i, nf);
    rho_a(i, nf)=abs(Zyx(i, nf))^2/(2*pi*fre(nf)*mu);
    phase(i, nf)=-atan(imag(Zyx(i, nf))/real(Zyx(i, nf)))*180/pi;
end
Hx=u_new;

```